

***Interactive comment on “The Influence of Assimilating Leaf Area Index in a Land Surface Model on Global Water Fluxes and Storages” by Xinxuan Zhang et al.***

**Anonymous Referee #2**

Report was submitted on 30 April 2020

**General comments**

This is the second time I am reviewing this manuscript, and thanks to the authors for taking into account of my previous comments. Authors did a fair job addressing my reviews, and the new version of the manuscript has been significantly improved. However, I still have an issue with the relationship between LAI and terrestrial water fluxed and storages variables (ET, CIE, CWS, SSM, TWS), at least in the section of discussion. The authors would pay more attention in the connection of LAI with these variables, or is there a relationship among the variables themselves? The paper has potential for publication in HESS after revisions.

The authors would like to thank the reviewer for their time and effort. As suggested, we have revised the Discussion section by adding a paragraph that investigates the relationships between LAI and water variables.

*As a key factor in land surface processes, precipitation greatly affects surface water fluxes and states and, consequently, affects the vegetation development. Furthermore, changes in vegetation also have considerable impact on the surface water condition. Sections 3.1 and 3.2 quantified changes in five water variables (ET, CIE, CWS, SSM, and TWS) due to the LAI assimilation in Noah-MP. Among the five variables, CIE and CWS are directly related to LAI, while the relationships between LAI and ET, SSM, and TWS are more complex (and indirect) and involve several other factors. For example, ET counts the water losses via both vegetation and soil; SSM is impacted by precipitation, temperature, soil characteristics, etc.; TWS considers all the water storage in the land surface and subsurface, including CWS and SSM.*

*The performance of the proposed LAI assimilation largely varies depending on the modeled variable, land cover type, errors in the model input (e.g., wet or dry bias in the forcing precipitation), and season. This is due to the complex relationships between vegetation and land water condition. Specifically, results in this study indicate that assimilating LAI in Noah-MP improves the model estimates of water fluxes and storages under positively biased precipitation input, but does not benefit most of the selected water variables when the precipitation input is characterized by a negative bias.*

1       **The Influence of Assimilating Leaf Area Index in a Land Surface**  
2                   **Model on Global Water Fluxes and Storages**

3

4   Xinxuan Zhang<sup>1</sup>, Viviana Maggioni<sup>1</sup>, Azbina Rahman<sup>1</sup>, Paul Houser<sup>1</sup>, Yuan Xue<sup>1</sup>, Timothy  
5   Sauer<sup>1</sup>, Sujay Kumar<sup>2</sup> and David Mocko<sup>2</sup>

6

7   1. George Mason University, Fairfax, VA, USA

8   2. Hydrological Sciences Laboratory, NASA Goddard Space Flight Center, Greenbelt, MD, USA

9

10

11

12

13

14

15

16

17

18

Submit to:

19

Hydrology and Earth System Sciences

20

May, 2020

21

22

## Abstract

23  
24 Vegetation plays a fundamental role not only in the energy and carbon cycles, but also in the global  
25 water balance by controlling surface evapotranspiration (ET). Thus, accurately estimating  
26 vegetation-related variables has the potential to improve our understanding and estimation of the  
27 dynamic interactions between the water, energy, and carbon cycle. This study aims to assess to  
28 what extent a land surface model (LSM) can be optimized through the assimilation of leaf area  
29 index (LAI) observations at the global scale. Two Observing System Simulation Experiments  
30 (OSSEs) are performed to evaluate the efficiency of assimilating LAI into an LSM through an  
31 Ensemble Kalman Filter (EnKF) to estimate LAI, ET, canopy interception evaporation (CIE),  
32 canopy water storage (CWS), surface soil moisture (SSM), and terrestrial water storage (TWS).  
33 Results show that the LAI data assimilation framework not only effectively reduces errors in LAI  
34 model simulations, but also improves all the modeled water flux and storage variables considered  
35 in this study (ET, CIE, CWS, SSM, and TWS), even when the forcing precipitation is strongly  
36 positively biased (extremely wet condition). However, it tends to worsen some of the modeled  
37 water-related variables (SSM and TWS) when the forcing precipitation is affected by a dry bias.  
38 This is attributed to the fact that the amount of water in the LSM is conservative and the LAI  
39 assimilation introduces more vegetation, which requires more water than what available within the  
40 soil.

41

## 42 **1. Introduction**

43 Terrestrial vegetation plays a vital role in the global water cycle, as it controls the surface  
44 evapotranspiration (ET) and the state of the carbon cycle. As shown in past literature, there exists  
45 a strong relationship among vegetation, precipitation, and soil moisture (Di et al., 1994; Farrar et  
46 al., 1994; Richard and Pocard, 1998; Adegoke and Carleton, 2002). Nevertheless, the role that  
47 vegetation and its dynamics play in the water cycle (for instance on the variability of precipitation)  
48 is extremely complex (Wang and Eltahir 2000; Wang et al. 2011). In the past half-century, these  
49 land surface processes and feedbacks have been examined through numerical modeling  
50 experiments (Foley et al. 1996; Kim and Wang 2007; Druel et al. 2019). In early generation land  
51 surface models (LSMs), the development stage of vegetation was prescribed by regularly updating  
52 vegetation variables, based on fixed lookup tables to simplify the model computation (Foley et al.  
53 1996). This approach uses constant vegetation indices, e.g., the leaf area index (LAI), while in  
54 reality the growth of vegetation continuously changes in response to weather and climate  
55 conditions. To overcome this deficiency, new generation LSMs are coupled with dynamic  
56 vegetation modules that comprehensively simulate several biogeochemical processes (Woodward  
57 and Lomas 2004; Gibelin et al. 2006; Fisher et al. 2018) and that are able to capture more detailed  
58 variations in plant productivity than traditional methods (Kucharik et al. 2000; Arora 2002;  
59 Krinner et al. 2005).

60 LAI can also be estimated through observations from satellite sensors, such as the  
61 Moderate Resolution Imaging Spectroradiometer (MODIS, Pagano and Durham 1993; Justice et  
62 al. 2002), the Système Probatoire d'Observation de la Terre VEGETATION (SPOT-VGT, Baret  
63 et al. 2007), and the National Oceanic and Atmospheric Administration (NOAA) Advanced Very  
64 High Resolution Radiometer (AVHRR, Cracknell 1997). LAI products retrieved from different

65 satellite missions and sensors provide spatially and temporally varying LAI fields on a routine  
66 basis at regional and global scales, including the MODIS LAI (Myneni et al. 2002), the Global  
67 Land Surface Satellite (GLASS) LAI (Xiao et al. 2013), and the GLOBMAP LAI dataset (Liu et  
68 al. 2012), among others. Satellite-derived LAI products were found to be affected by uncertainties  
69 due to the limitation of retrieval algorithms and vegetation type sampling issues (Cohen and Justice  
70 1999; Privette et al. 2002; Tian et al. 2002; Morisette et al. 2002).

71 A method to combine the inherently incorrect estimates from satellite observations and  
72 model simulations is data assimilation (DA). One of the most common DA systems — the  
73 Ensemble Kalman Filter (EnKF; Evensen 2003) — dynamically updates the model error  
74 covariance information by producing an ensemble of model predictions, which are individual  
75 model realizations perturbed by the assumed model error (Reichle et al. 2007). The ensemble  
76 approach is widely used in hydrology because of its flexibility with respect to the type of model  
77 error (Crow and Wood 2003) and well suited to the nonlinear nature of land surface processes  
78 (Reichle et al. 2002a, 2002b; Andreadis and Lettenmaier 2006; Durand and Margulis 2008; Kumar  
79 et al. 2008; Pan and Wood 2006; Pauwels and De Lannoy 2006; Zhou et al. 2006). However, the  
80 use of an EnKF for the assimilation of LAI in LSMs has not been thoroughly investigated in the  
81 past. Pauwels et al. (2007) proposed an Observing System Simulation Experiment (OSSE) to  
82 evaluate the performance of assimilating LAI in a hydrology-crop growth model with an EnKF  
83 algorithm. Other studies have also tested simplified 1D-VAR and extended Kalman filter methods  
84 for LAI assimilation (e.g., Sabater et al. 2008; Barbu et al. 2011; Fairbairn et al. 2017). Recently,  
85 Kumar et al. (2019) assimilated GLASS LAI in a land surface model with an EnKF across the  
86 continental U.S. Some water budget variables were improved through the assimilation procedure,  
87 particularly in agricultural areas where the assimilation added harvesting information to the model.

88 Ling et al. (2019) assimilated global LAI information with an Ensemble Adjust Kalman Filter  
89 (EAKF) algorithm and found that the assimilation is more effective during the growing season.  
90 LAI assimilation also had a positive impact on gross primary production (GPP) and ET in low  
91 latitude regions.

92 Nevertheless, most of the aforementioned studies mainly focused on the impact of LAI  
93 assimilation on the simulated LAI or vegetation biomass. Only a few studies discussed the  
94 influences of LAI assimilation on the estimation of water variables such as soil moisture or  
95 streamflow (Pauwels et al. 2007; Sabater et al. 2008) and most of them focused on limited regions.  
96 Most recently, Albergel et al. (2017) conducted a study on a much larger domain – Europe and the  
97 Mediterranean basin –and showed improvement in soil moisture at various depths thanks to LAI  
98 assimilation.

99 This work leverages upon these studies but aims to assess to what extent a land surface  
100 model, especially the simulation of water-related variables, can be optimized through the  
101 assimilation of LAI observations at the global scale. As this study serves as a feasibility test to  
102 quantify the impact of LAI assimilation on water cycle variables, an OSSE is chosen to investigate  
103 the model’s behavior. This guarantees that reference variables (often referred to as the “truth”),  
104 which are synthetically produced, are available for quantifying the performance of the proposed  
105 framework. Specifically, two OSSEs that apply an EnKF algorithm to the Noah LSM with multi-  
106 parameterization options (Noah-MP, Niu et al. 2011; Yang et al. 2011) are performed to evaluate  
107 the efficiency of assimilating LAI observations for estimating ET, canopy interception evaporation  
108 (CIE), canopy water storage (CWS), surface soil moisture (SSM), and terrestrial water storage  
109 (TWS).

110

111

## 112 **2. Methods and materials**

### 113 ***2.1. Land surface model (Noah-MP)***

114 The Noah-MP 3.6 (Niu et al. 2011; Yang et al. 2011) is adopted in this study. Noah-MP contains  
115 a separate vegetation canopy defined by a canopy top and bottom, crown radius, and leaves with  
116 defined dimensions, orientation, density, and radiometric properties (Niu et al. 2011). Multiple  
117 options are available for surface water infiltration, runoff, groundwater transfer and storage  
118 including water table depth to an unconfined aquifer (Niu et al. 2007), dynamic vegetation, canopy  
119 resistance, and frozen soil physics. Specifically, the prognostic vegetation growth combines a Ball-  
120 Berry photosynthesis-based stomatal resistance (Ball et al. 1987) with a dynamic vegetation model  
121 (Dickinson et al. 1998). The dynamic vegetation model calculates the carbon storages in various  
122 parts of the vegetation (leaf, stem, wood, and root) and the soil carbon pools.

123 The Noah-MP 3.6 LSM has been implemented into the National Aeronautics and Space  
124 Administration (NASA) Land Information System (LIS; Peters-Lidard et al. 2007; Kumar et al.  
125 2006). LIS is a software that provides an interagency test bed for land surface modeling and data  
126 assimilation that allows customized systems to be built, assembled and reconfigured easily, using  
127 shared plugins and standard interfaces. All the experiments in this study are setup through LIS.  
128 The Modern-Era Retrospective analysis for Research and Applications Version 2 (MERRA-2;  
129 Gelaro et al. 2017) dataset serves as the meteorological forcings of Noah-MP. MERRA-2 is the  
130 latest atmospheric reanalysis produced by the NASA Global Modeling and Assimilation Office  
131 (GMAO) and includes updates from the Goddard Earth Observing System (GEOS). The  
132 meteorological variables selected from MERRA-2 include surface pressure, surface air  
133 temperature, surface specific humidity, incident radiations, wind speed, and precipitation rate.

134 Five model output variables that describe terrestrial water fluxes and storages are  
135 investigated in this work: ET (defined as the sum of evaporation and the plant transpiration  
136 [kg/m<sup>2</sup>s]), CIE (defined as the evaporation of the canopy intercepted water [kg/m<sup>2</sup>s]), CWS  
137 (defined as the amount of canopy intercepted water in both liquid and ice phases [kg/m<sup>2</sup>]), SSM  
138 (defined as the water content in the top 10 cm of the soil column [m<sup>3</sup>/m<sup>3</sup>]), and TWS (defined as  
139 the sum of all water storage on the land surface and in the subsurface [mm]).

140

## 141 *2.2. Experimental design*

142 An OSSE is designed to understand the efficiency of assimilating LAI within Noah-MP version  
143 3.6 using a one-dimensional EnKF algorithm (Reichle et al. 2010), when the precipitation forcing  
144 data are strongly biased. Being the major driving force of the hydrological cycle, the quality of  
145 input precipitation is critical for the accuracy of land surface model outputs. However, global  
146 precipitation datasets are far from being perfect and often affected by large regional biases. For  
147 example, the MERRA-2 precipitation dataset shows a widespread relative bias greater than 100%  
148 in South Asia (Ghatak et al. 2018). Although an EnKF is optimal only under the assumption of  
149 unbiasedness (which is not met in the proposed experimental setup), we want to investigate here  
150 to what extent the EnKF LAI assimilation (even if sub-optimal) can improve water storages and  
151 fluxes under two extreme conditions, i.e., a very dry and a very wet precipitation bias, knowing  
152 that such biases are very plausible in the real world and often unknown (and therefore difficult to  
153 remove). The proposed framework is evaluated through a global experiment (Antarctica excluded)  
154 at the  $0.625^\circ \times 0.5^\circ$  spatial resolution of the MERRA-2 forcing dataset (Figure 1).



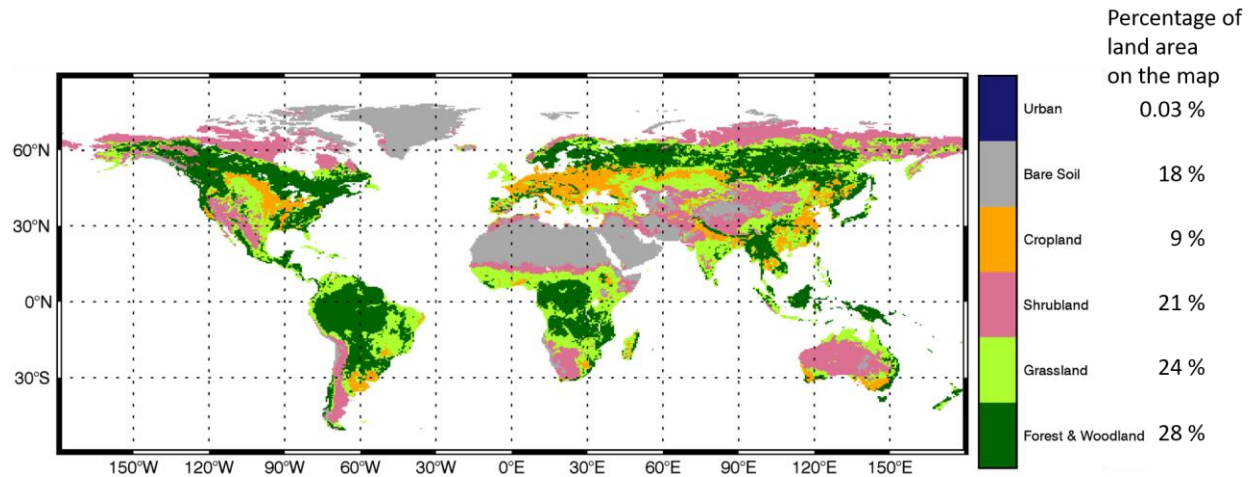


Figure 1. Study domain and land cover types (Hansen et al. 2000).

155

156

157

158

159

160

161

162

163

164

165

166

167

168

169

170

171

Figure 2 shows a schematic diagram of the experiments. First, the Noah-MP model is spun-up for a 10-year period (2001-2010) to ensure a physically realistic state of equilibrium. Second, the model is run for a 29-month period (January 2011 – May 2013) to conduct the Nature Run (NR) with the same configuration as the spin-up one. By definition, an OSSE is a controlled experiment that does not assimilate any real observation. Instead, it treats all the model outputs from the NR as the “true” condition (denoted as the “synthetic truth”). The “true” LAI (i.e., the LAI output from NR) is then perturbed via a simple additive error model to produce the synthetic observations to be assimilated into the DA runs. The spin-up run and NR are forced by the original MERRA-2 precipitation data. Third, two Open Loop (OL) runs (no DA) are conducted for the same 29-month period under two conditions: i) “extremely dry” condition (the model is forced by halving the MERRA-2 precipitation data; OL-dry), and ii) “extremely wet” condition (the model is forced by doubling the MERRA-2 precipitation; OL-wet). The biased forcing precipitation data in OL mimic typical precipitation biases in current precipitation reanalysis and satellite products (e.g., Ghatak et al. 2018; Yoon et al. 2019).

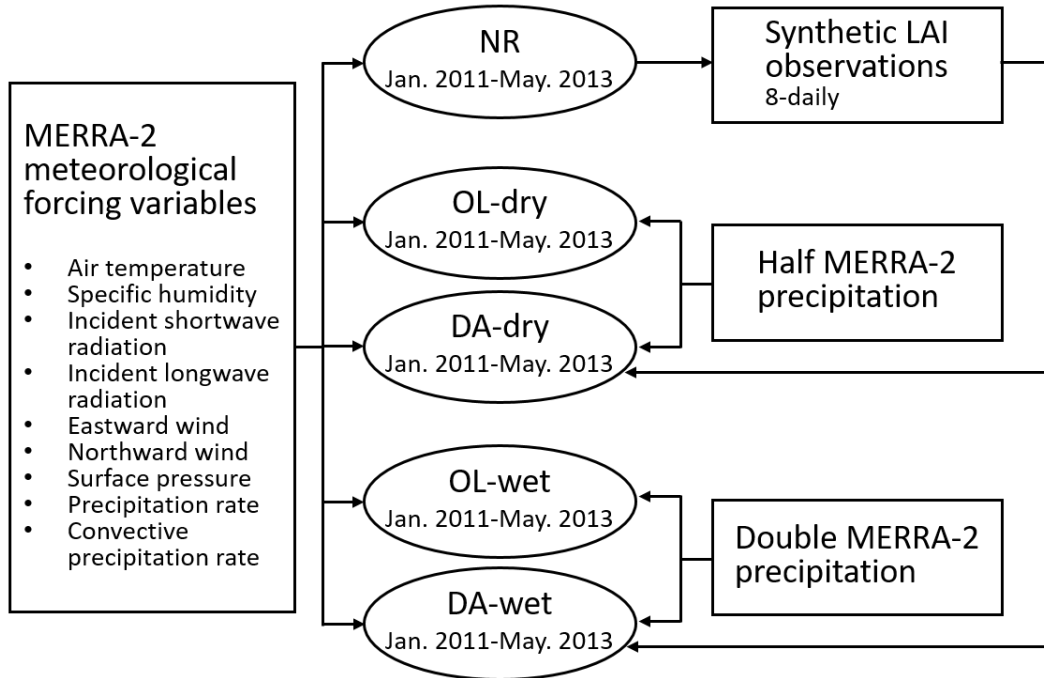


Figure 2. Schematic diagram of the OSSE design.

172

173

174

175 The two DA runs are then conducted under the two same conditions (DA-dry and DA-wet)  
 176 using a one-dimensional EnKF assimilation algorithm, which is a built-in DA method in LIS. The  
 177 EnKF DA algorithm is suitable for non-linear and intermittent land surface processes (Reichle et  
 178 al. 2002a, 2002b). Details of the algorithm can be found in numerous previous studies (Reichle et  
 179 al. 2010; De Lannoy et al. 2012; Liu et al. 2015; Kumar et al. 2019a).

180 The model ensemble is generated by perturbing a set of meteorological forcing. To select  
 181 the optimal ensemble size, a sensitivity test is performed for ensemble sizes spanning from 2 to 24  
 182 members (not shown here). The number of ensemble members has a strong impact on the model  
 183 results at small sizes, while the model performance tends to become steady when more than 20  
 184 ensemble members are considered. Thus, all the DA simulations are run for 20 members.

185 The synthetic LAI observations are obtained from the NR and assimilated to the DA system  
 186 at 8-daily frequency. The synthetic LAI observation has the same temporal resolution as the

187 MODIS LAI product but with full coverage over the study domain. In real case studies, satellite  
188 LAI products contain a substantial amount of missing data, mainly due to the cloud obscuration  
189 gaps. Based on the vegetation type in the model, the leaf mass fields are also updated. Random  
190 perturbations of MERRA-2 meteorological forcings and synthetic LAI observations are applied to  
191 create an ensemble of land surface conditions that represent the uncertainties of in the LSM.

192         Similar to previous work (Kumar et al. 2014, 2019a, 2019b), the MERRA-2 forcing inputs  
193 such as shortwave/longwave radiations and precipitation are perturbed hourly. Multiplicative  
194 perturbations are applied to the shortwave radiation and precipitation with a mean of 1 and standard  
195 deviations of 0.3 and 0.5, respectively. The longwave radiation is perturbed via an additive  
196 perturbation with a standard deviation of  $50 \text{ W/m}^2$ . The perturbations of the three meteorological  
197 forcing variables also include cross correlations: cross correlation between shortwave radiation  
198 and precipitation is -0.8, cross correlation between longwave radiation and precipitation is 0.5; and  
199 cross correlation between shortwave and longwave radiations is -0.5. The synthetic LAI  
200 observations are perturbed via an additive model with a standard deviation of 0.1.

201

### 202 ***2.3. Evaluation and error metrics***

203 Output variables from the OL and DA runs are evaluated against the “truth” from the NR at daily,  
204 monthly, and seasonal temporal scales. Besides LAI, five more water fluxes and storages are  
205 evaluated in the results section: ET, CIE, CWS, SSM, and TWS.

206         The initial condition for the OL and DA runs is generated by a spin-up run that uses the  
207 original MERRA-2 precipitation as input. However, the OL and DA runs are forced by either  
208 doubled or halved precipitation, which is not consistent with the spin-up run and the model needs  
209 some time to stabilize. The first 5-month model outputs are therefore eliminated from the

210 evaluation to avoid the model systematic instability at the beginning of the OL and DA simulations  
 211 and the evaluation, thus, focused only on model outputs from 2011-06-01 to 2013-05-31. Results  
 212 are discussed using maps and time series of global averaged values and anomalies. Each of the  
 213 anomaly time series is computed relative to the mean of its respective model run. Moreover, two  
 214 error metrics are employed to quantify the difference between OL (and DA) with respect to the  
 215 reference variables (from the NR). The first one is the Normalized and Centered Root Mean Square  
 216 Error (NCRMSE), defined as follows:

$$217 \quad E = \frac{\left\{ \frac{1}{N} \sum_{i=1}^N [(X_i - \text{mean}(X)) - (O_i - \text{mean}(O))]^2 \right\}^{\frac{1}{2}}}{\text{mean}(O)} \quad \text{Eq. 1}$$

218 where  $E$  is the NCRMSE,  $O$  is the NR output variable, and  $X$  is the output variable from the OL  
 219 runs or DA runs.  $N$  is the total number of  $X$  values, and  $i$  represents the index of each  $X$  value.  
 220 Second, to investigate the improvement (or degradation) due to the DA of LAI observations, we  
 221 adopt the Normalized Information Contribution (NIC, similar to the NIC in Kumar et al. 2016)  
 222 index based on NCRMSE and defined as:

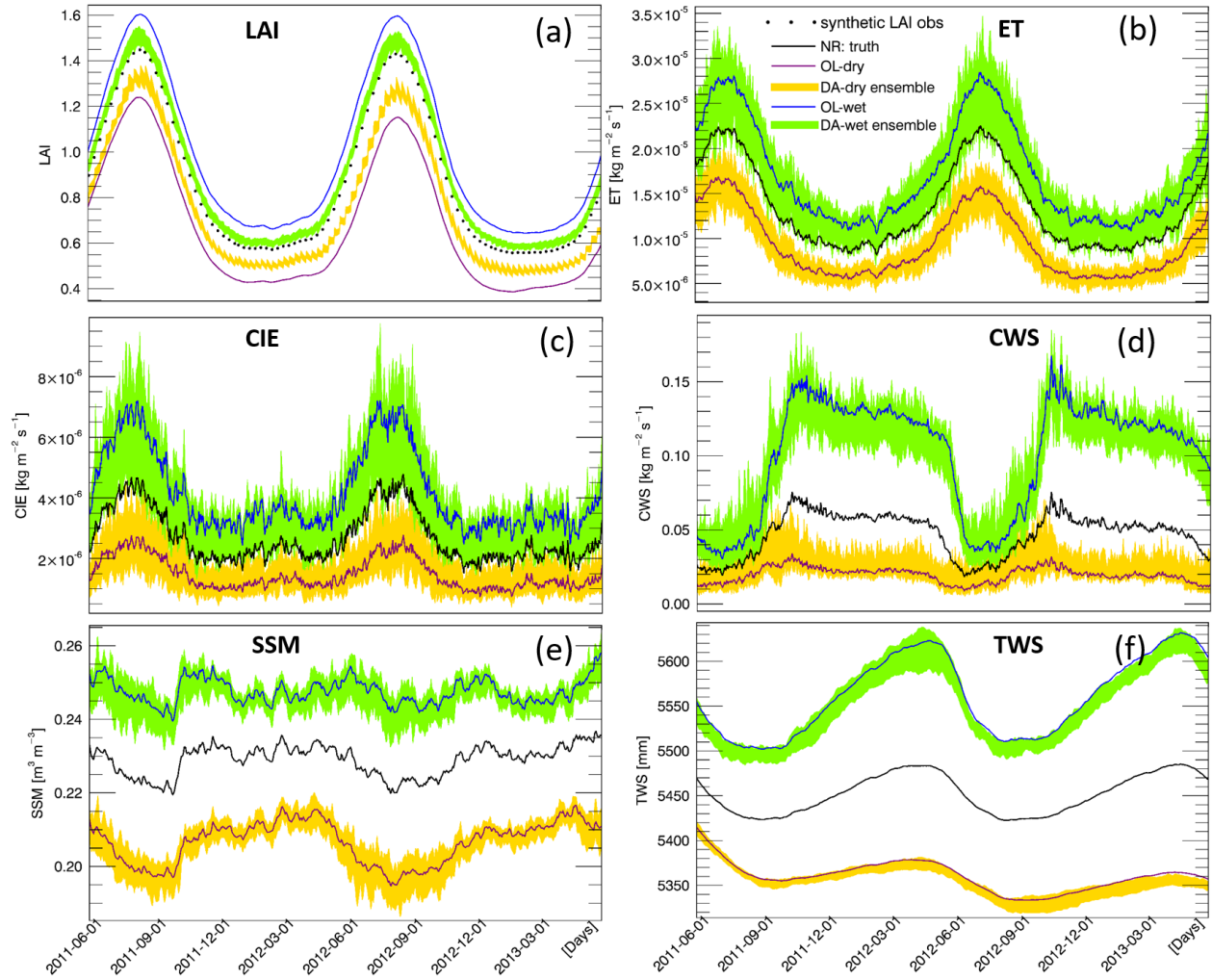
$$223 \quad C = \frac{E_{DA} - E_{OL}}{0 - E_{OL}} \quad \text{Eq. 2}$$

224 where  $C$  represents the NIC index and  $E$  is the NCRMSE for OL or DA runs. NIC equals to 1  
 225 means that DA realizes the maximum possible improvement over the OL; NIC equals to zero  
 226 means that DA and OL show the same performance skills; and negative NIC indicates a model  
 227 degradation through DA.

228

### 229 **3. Results and discussion**

#### 230 **3.1. LAI**

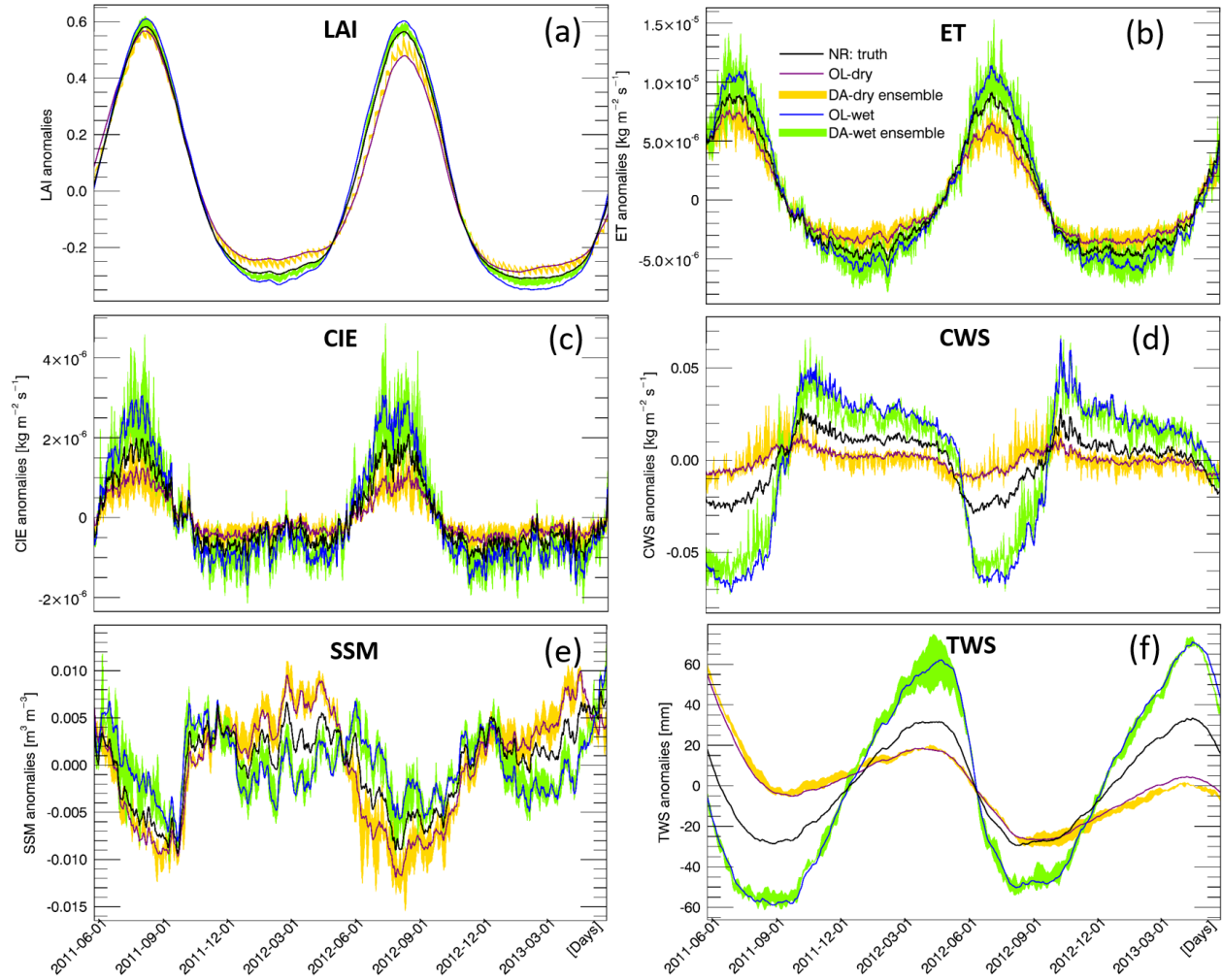


231

232

Figure 3. Global averaged daily values of LAI and five water variables (2011-06-01 to 2013-05-30).

233



234

235

Figure 4. Global averaged daily anomalies of LAI and five water variables (2011-06-01 to 2013-05-30).

236

237 Figure 3a and Figure 4a show time series of global averaged LAI values and corresponding

238 anomalies, respectively. As expected, LAI values are largely impacted by the extreme precipitation

239 conditions. The wet condition introduces more vegetation, while the dry condition limits the

240 vegetation growth throughout the two-year period. The DA procedure effectively corrects the LAI

241 errors caused by the biased precipitation input. The seasonality of LAI anomalies is evident,

242 showing larger variations in DJF and JJA than during the transition periods (MAM and SON). The

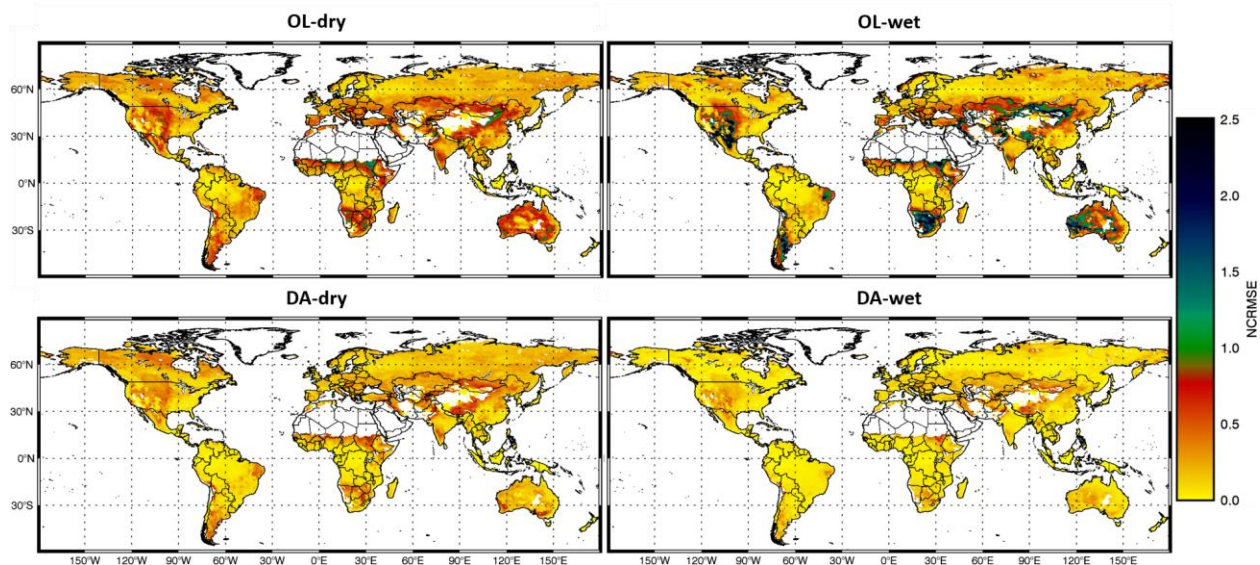
243 OL-wet condition simulation shows larger LAI anomalies than the NR reference, while the OL-

244 dry condition has smaller LAI anomalies than NR. The LAI anomalies obtained from DA runs  
245 under both wet and dry conditions are closer to the reference anomalies than the corresponding  
246 OL runs. In general, DA performs better in the wet condition experiment than in the dry case.  
247 Moreover, the DA runs show lower NCRMSEs than the corresponding OL runs across the globe  
248 (Figure 5a), especially over shrublands and grasslands (refer to Figure 1 for land covers).

249 In order to illustrate how LAI assimilation performs for different seasons, Figure 6a and  
250 Figure 7a show monthly averages of NCRMSE for LAI across the northern and southern  
251 hemispheres, respectively. In the northern hemisphere (Figure 6a), the NCRMSE time series  
252 follow clear seasonal patterns. First, the NCRMSE is higher in DJF/MAM and is lower in JJA/SON  
253 for both extreme precipitation conditions. The highest NCRMSE values are in March and April,  
254 and the lowest values are in July, August, and September. The differences of NCRMSE between  
255 OL and the corresponding DA runs tend to be much larger in MAM than in any other seasons,  
256 which means that LAI assimilation is more effective in the vegetation growth period. Moreover,  
257 the NCRMSE is constantly higher in the dry condition runs than the wet ones, which is due to the  
258 fact that the growth of vegetation is sensitive to the lack of water. Differences between wet and  
259 dry conditions are much smaller in JJA than in other seasons. In JJA, the vegetation leaves in the  
260 north hemisphere are fully developed and the plants can use stomatal closure to preserve water  
261 under water limited condition (dry condition). Thus, the NCRMSE of dry condition becomes  
262 smaller and does not show much difference from the wet condition. The southern hemisphere  
263 (Figure 7a), which does not have a strong climate seasonality, shows more modest seasonal  
264 NCRMSE patterns than the northern regions. In general, the NCRMSEs in the southern  
265 hemisphere are smaller than the ones in the northern hemisphere all year around. Specifically,

266 NCRMSEs in the southern hemisphere are slightly higher in October, November, and December,  
267 when the differences between OL and DA runs are also larger.

268



269

270 Figure 5. Maps of LAI NCRMSE for the OL and DA runs.

270

271

### 272 3.2. Water fluxes and storages

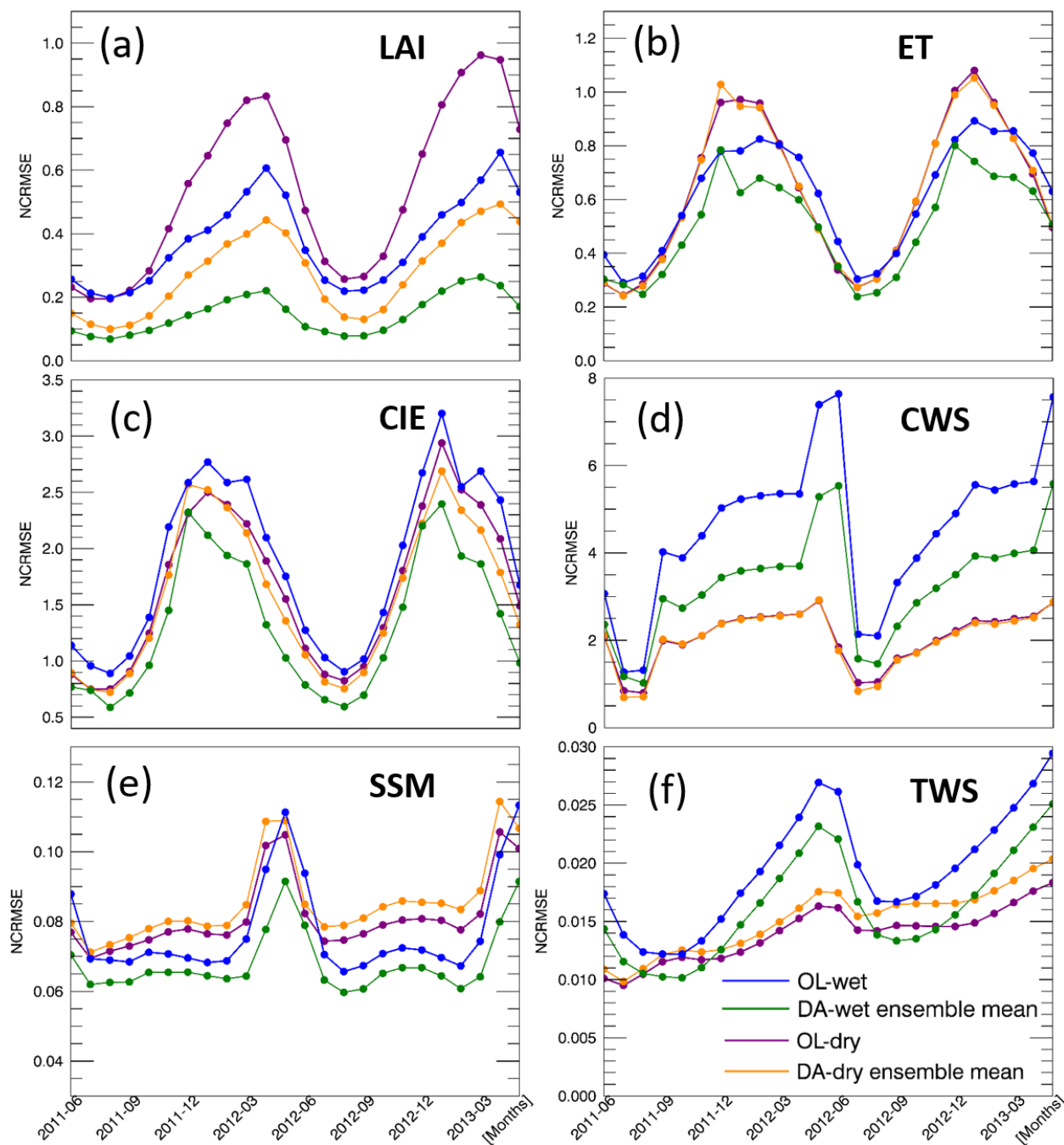
273 As mentioned in section 2.3, we focus on five water-related variables from the Noah-MP output  
274 to evaluate the impact of LAI assimilation on simulating the water cycle (ET, CIE, CWS, SSM,  
275 and TWS). Daily time series of global averaged values and corresponding anomalies of the five  
276 water variables are shown in Figure 3(b-f) and Figure 4(b-f), respectively. The model well  
277 simulates the seasonality of all water fluxes/storages considered here. The OL runs reveal that  
278 global average values of all five variables are impacted by the highly biased precipitation  
279 conditions. The variations of anomalies for ET, CIE, CWS, and TWS tend to be amplified by the  
280 wet condition and tend to be dampened by the dry condition. On the contrary, the anomalies of  
281 SSM become larger in dry conditions and become smaller in wet conditions, which is probably



282 due to the limited soil water capacity. The surface soil is more likely to get saturated in wet  
283 conditions when the precipitation doubles the original amount, but SSM cannot get larger once the  
284 soil is saturated, even if there is more precipitation added to the system. Thus, the range of SSM  
285 anomalies in the wet experiment is limited and narrower than in the dry condition. The green and  
286 yellow shaded areas represent the ensemble of the DA runs. The anomaly ensembles of the five  
287 water variables show slight improvements through DA when precipitation is severely positively  
288 biased (wet condition). However, none of these variables shows improvement when the  
289 precipitation is severely negatively biased (dry condition) – the anomalies either have no change  
290 through the LAI DA (ET, CIE, and CWS) or worsen the OL-dry run (SSM and TWS).

291 To further investigate the efficiency of assimilating LAI in Noah-MP, time series of  
292 monthly NCRMSE averages are shown in Figure 6(b-f) and Figure 7(b-f) for all five water  
293 variables. The five variables can be divided into two main groups based on their performances:  
294 ET/CIE/CWS and SSM/TWS. For the wet bias experiment, DA improves the NCRMSE for all  
295 variables. However, LAI assimilation is not able to correct the model when the input precipitation  
296 is negatively biased (dry condition). A dry precipitation bias means that the system has  
297 (erroneously) less water than in reality (NR in the synthetic experiment). Since no water is  
298 otherwise added to the system, LAI DA cannot fully correct water-related model states (such as  
299 soil moisture). The NCRMSEs of DA runs are either the same as in the OL runs (ET/CIE/CWS)  
300 or worse (SSM/TWS). Specifically, ET/CIE/CWS have larger NCRMSE in the northern  
301 hemisphere and much smaller NCRMSEs in the southern hemisphere, but SSM/TWS do not show  
302 large differences between north and south. Moreover, ET/CIE/CWS in the northern hemisphere  
303 follow a seasonal pattern: NCRMSEs are lower in warm season (JJA) and higher in the colder  
304 season (DJF and March). In the southern hemisphere the three variables also have relative higher

305 NCRMSE in the colder season (JJA). On the contrary, SSM/TWS show a different seasonal pattern  
 306 that NCRMSEs are larger in the warmer season (April, May, and June) over northern hemisphere.  
 307 In southern hemisphere, TWS also has larger NCRMSEs in warmer season (October to April), but  
 308 SSM shows higher NCRMSEs in colder season (similar to the ET/CIE/CWS group).



309  
 310 Figure 6. Monthly averaged NCRMSE for LAI and five water variables over the Northern hemisphere.

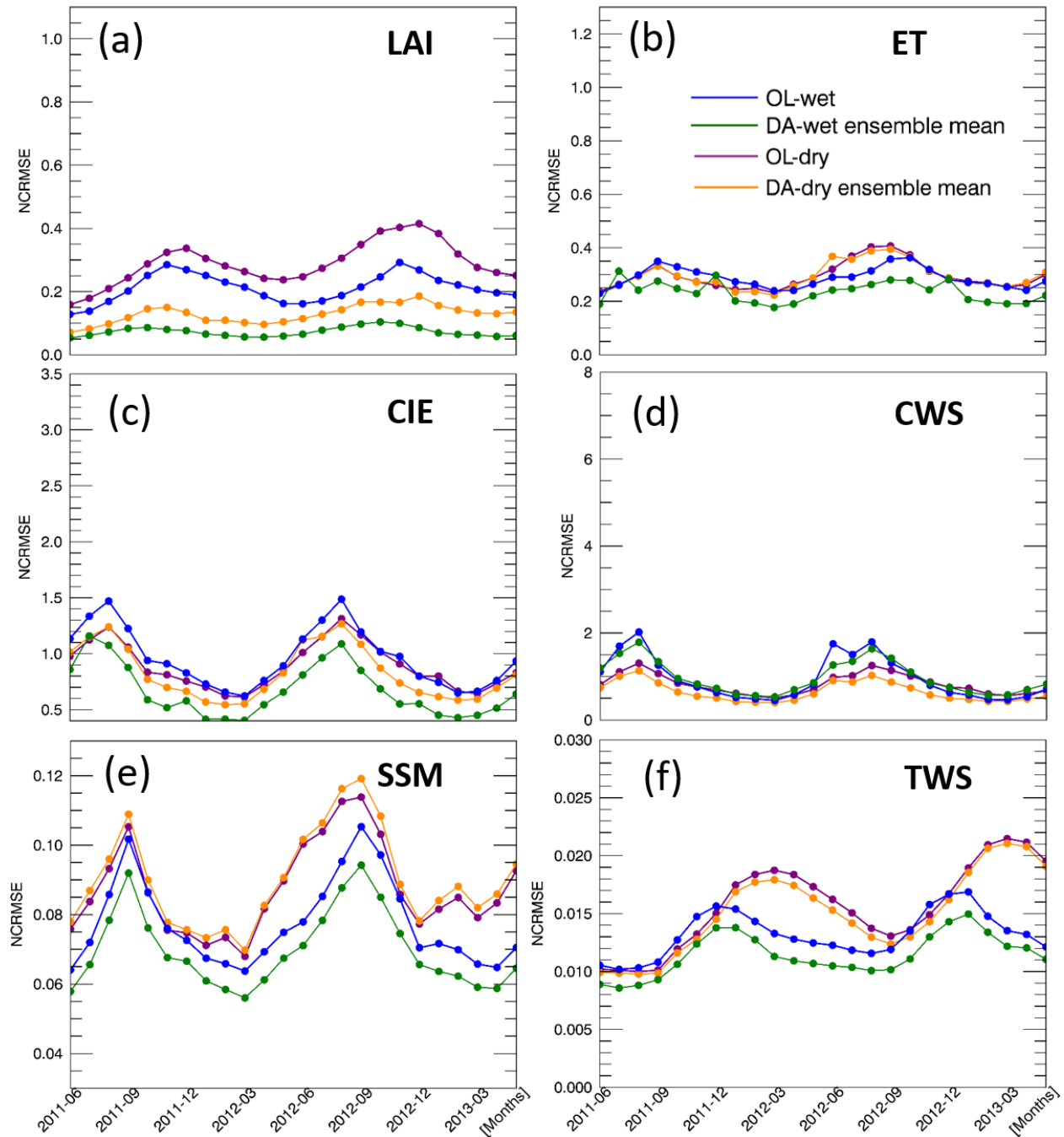


Figure 7. Same as in Figure 6, but for the Southern hemisphere.

311

312

313

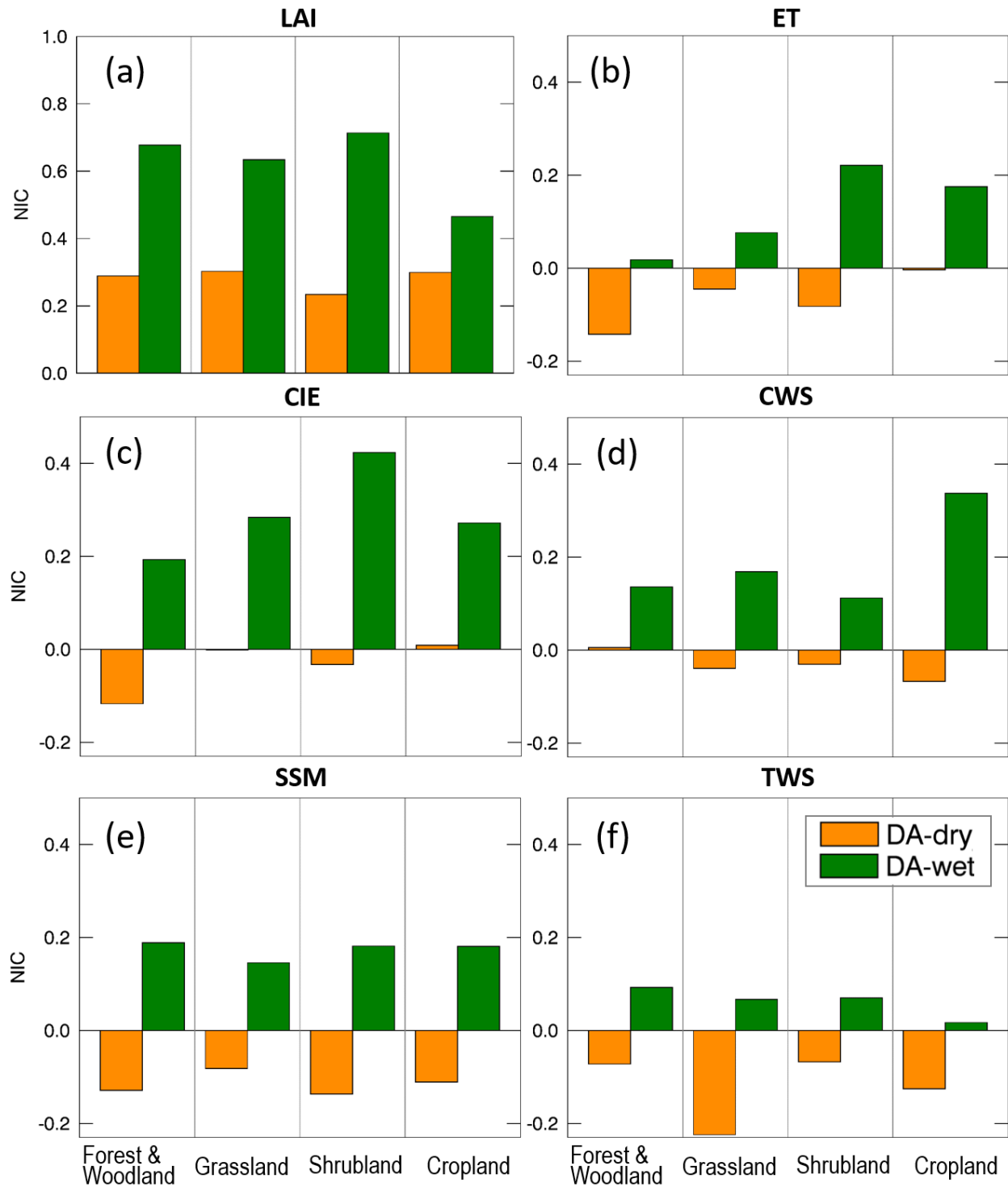
314 The improvements in the model water fluxes and storages through LAI DA are also

315 quantified by the NIC index (defined in Eq. 2). Figure 8 presents comparisons among NIC indices

316 for each water variable analyzed in this study across areas with four different land cover types:

317 forest & woodland, grassland, shrubland, and cropland. In general, LAI DA improves the NIC  
318 indices with positively biased input precipitation (DA-wet) but worsens the NIC when negatively  
319 biased input precipitation (DA-dry) is considered. Specifically, in wet condition, ET, CIE, and  
320 CWS have higher variability over areas with different land cover types, while SSM and TWS have  
321 similar NIC values across different land covers. Shrubland and cropland tend to perform better in  
322 wet condition except for TWS. In dry condition, the NICs of ET, CIE, and TWS have higher  
323 variability than the ones of CWS and SSM. SSM and TWS show very low NIC values in dry  
324 condition for almost all land covers. Overall the NIC values of ET, CIE, and CWS are better than  
325 the ones of SSM and TWS for all land cover types, though the NICs of ET and CIE over forest &  
326 woodland perform very poorly.

327

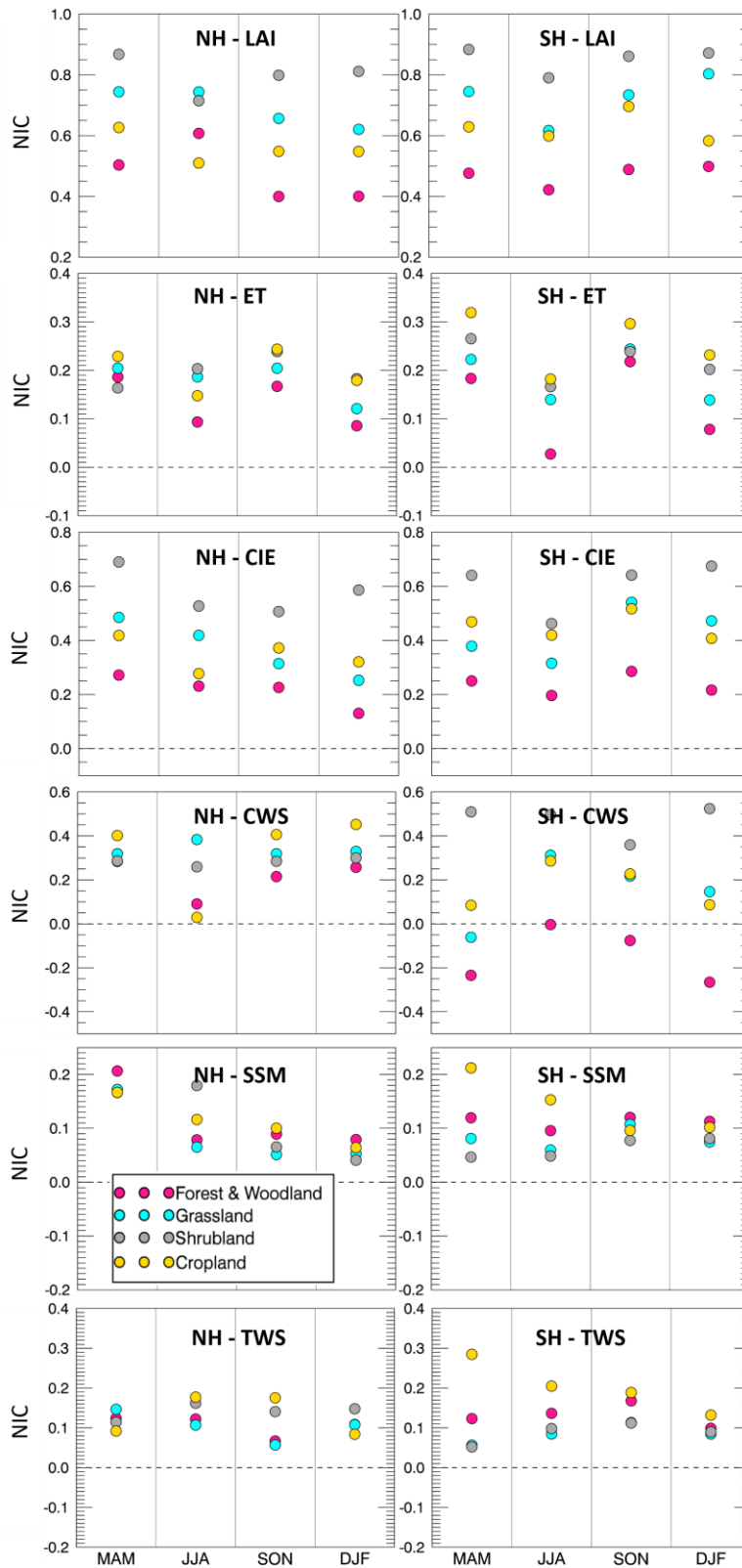


328

329

Figure 8. NIC for different variables and different land cover types for the two DA runs.

330

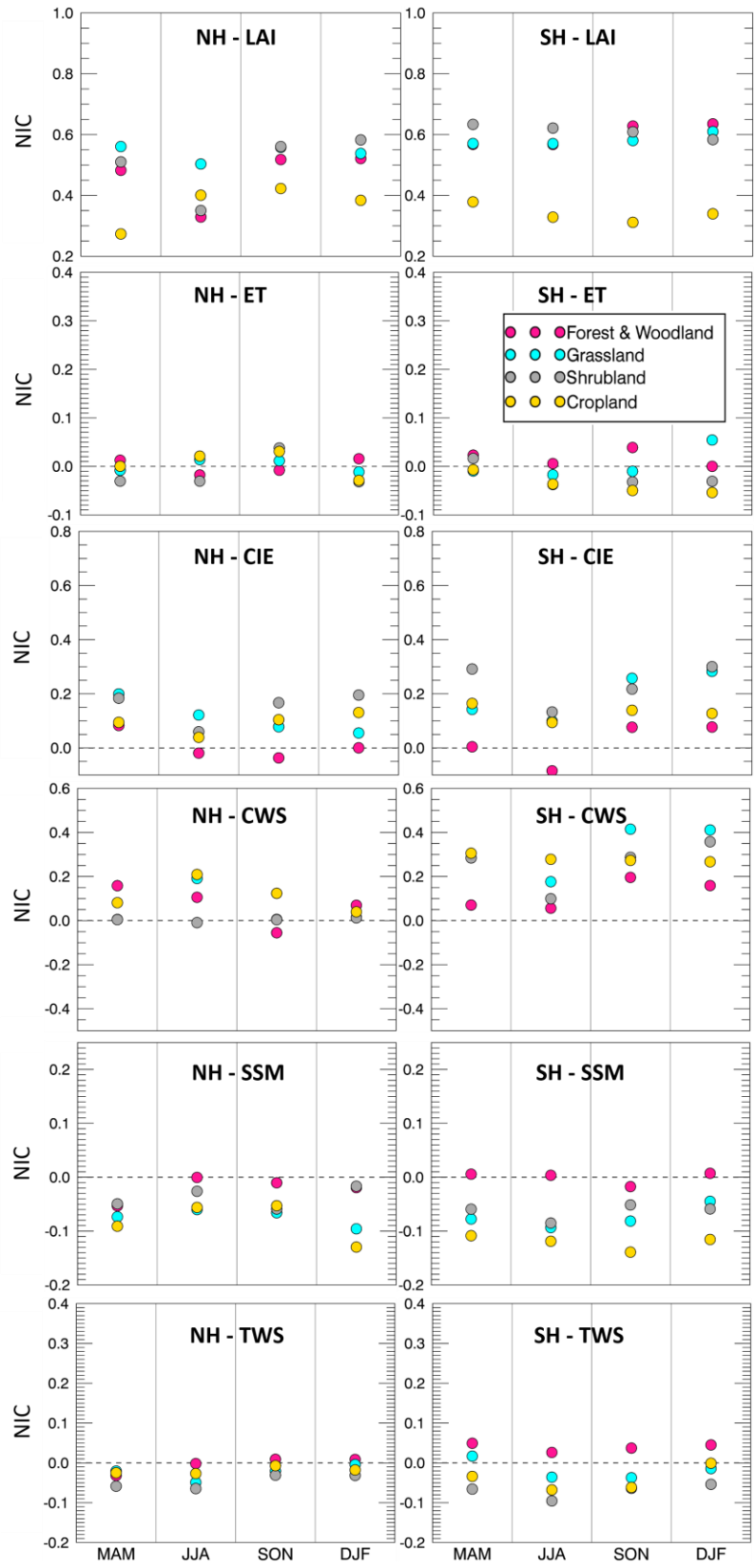


331  
332

Figure 9. NIC of five water variables under wet precipitation conditions over northern and southern hemispheres

333

(NH and SH) during different seasons (MAM, JJA, SON, and DJF)



334

335

Figure 10. Same as in Figure 9, but for the dry precipitation experiment.

336

337           The effectiveness of LAI DA therefore varies across the northern and southern hemispheres,  
338 different land cover types, as well as different input precipitation biases. To further investigate the  
339 influence of LAI assimilation, Figures 8 and 9 present NIC values for each hemisphere, each  
340 season, and each of the input precipitation conditions – wet and dry, respectively. For the wet case  
341 (Figure 9), NIC is positive in most cases, which means that the five water variables benefit from  
342 the LAI assimilation in all seasons and in both hemispheres. The only exception is CWS which  
343 has negative NIC values in the southern hemisphere over grassland (in MAM season) and over  
344 forest & woodland (in all seasons). In fact, the forest & woodland region tends to have the least  
345 improvement through the LAI assimilation among all land cover types. This is probably because  
346 forests and woodlands have large water-holding capacity; thus, the change of water amount caused  
347 by LAI DA is not enough to improve the water-related variables. In other words, forest and  
348 woodland tend to have lower sensitivity in response to the change of precipitation conditions  
349 because of their large rooting depth. On the contrary, cropland is very sensitive to precipitation  
350 and it benefits the most from the assimilation of LAI for most of the variables. Moreover, NICs of  
351 ET/CIE/CWS tend to be smaller than the NICs of SSM and TWS. There is no clear seasonality in  
352 the NIC values, though it has a weak tendency to be lower in warm seasons.

353           For the dry condition case (Figure 10), NIC values are much lower than in the wet bias  
354 case. Nearly half of the NIC values for the five water-related variables are negative, meaning that  
355 DA degrades the OL estimates. Nevertheless, the forest & woodland regions tend to perform better  
356 than other land covers in dry condition for SSM and TWS. This is due to large soil reservoir of  
357 forests and woodlands, which keeps the model water storage more stable when the input  
358 precipitation is affected by large negative biases.



359

### 360 **3.3. Discussion**

361 As a key factor in land surface processes, precipitation greatly affects surface water fluxes and  
362 states and, consequently, affects the vegetation development. Furthermore, changes in vegetation  
363 also have considerable impact on the surface water condition. Sections 3.1 and 3.2 quantified  
364 changes in five water variables (ET, CIE, CWS, SSM, and TWS) due to the LAI assimilation in  
365 Noah-MP. Among the five variables, CIE and CWS are directly related to LAI, while the  
366 relationships between LAI and ET, SSM, and TWS are more complex (and indirect) and involve  
367 several other factors. For example, ET counts the water losses via both vegetation and soil; SSM  
368 is impacted by precipitation, temperature, soil characteristics, etc.; TWS considers all the water  
369 storage in the land surface and subsurface, including CWS and SSM.

370 The performance of the proposed LAI assimilation largely varies depending on the  
371 modeled variable, land cover type, errors in the model input (e.g., wet or dry bias in the forcing  
372 precipitation), and season. This is due to the complex relationships between vegetation and land  
373 water condition. Specifically, results in this study indicate that assimilating LAI in Noah-MP  
374 improves the model estimates of water fluxes and storages under positively biased precipitation  
375 input, but does not benefit most of the selected water variables when the precipitation input is  
376 characterized by a negative bias.

377 ~~Results presented in sections 3.1 and 3.2 indicate that assimilating LAI in Noah-MP~~  
378 ~~improves the model estimates of water fluxes and storages under positively biased precipitation~~  
379 ~~input, but does not benefit most of the selected water variables when the precipitation input is~~  
380 ~~characterized by a negative bias.~~

381 In the dry condition runs, Noah-MP is fed by only half of the original MERRA-2  
382 precipitation used in the NR. Considering that the amount of water in Noah-MP is conservative  
383 (since based on a water balance equation), the model has no additional water source in the system,  
384 even though the LAI assimilation pushes the model towards more vegetation (that should result in  
385 more water). As a matter of fact, introducing more vegetation in the system results in more ET and  
386 more root water uptake from the soil, which is most likely the cause for the poor performance of  
387 most water fluxes and storages in the DA-dry experiment.

388 On the other hand, the LAI assimilation is found to improve the original OL runs when the  
389 input precipitation is positively biased. This is because LAI assimilation is able to help constrain  
390 the partitioning of model water storage when there is abundant water in the system, thus, improving  
391 the performance of water-related variables. In summary, although the EnKF is run here in a sub-  
392 optimal mode (not satisfying the unbiasedness assumption), the assimilation of LAI is shown to  
393 have a positive impact on multiple variables and in several regions of the world.

394 Overall the improvement of water variables through LAI assimilation is not remarkable  
395 enough to compensate the model degradation caused by the biased precipitation forcing data.  
396 Previous studies (Pauwels et al. 2007; Sabater et al. 2007; Barbu et al. 2011; Fairbairn et al. 2017;  
397 Albergel et al. 2017) have tested the performance of the joint assimilation of LAI and soil moisture  
398 over regional domains and showed promising results. However, no experiment was performed at  
399 the global scale. Future work could investigate a multi-variate data assimilation system that  
400 concurrently merges both LAI and soil moisture (or TWS) observations globally.

401

## 402 **4. Conclusions**

403 This study evaluates the efficiency of assimilating vegetation information (i.e., LAI synthetic  
404 observations) within a land surface model (Noah-MP 3.6) when the precipitation forcing data are  
405 strongly biased (either positively or negatively). Two OSSEs that use an EnKF algorithm for LAI  
406 assimilation are performed at global scale during June 2011 – May 2013. The experiments use  
407 MERRA-2 as meteorological forcing data. The OL and DA runs are evaluated against a synthetic  
408 “truth” from a nature run, in which the MERRA-2 precipitation is neither perturbed nor biased.  
409 The performance of the proposed framework is evaluated for several model output, including LAI  
410 estimates and five water-related variables (ET, CIE, CWS, SSM, and TWS).

411 Overall the EnKF LAI assimilation procedure effectively reduces the LAI error under  
412 positively (wet case) and the negatively (dry case) biased precipitation conditions. For the five  
413 selected water flux or storage variables, LAI DA improves the model estimates when the model  
414 input precipitation is positively biased, but tends to worsen the OL estimates for some of those  
415 variables when the input precipitation is negatively biased. Specifically, SSM and TWS estimates  
416 are degraded in the DA-dry run with respect to the OL-dry run, while ET, CIE, and CWS do not  
417 present large changes when LAI is assimilated in the dry bias run. The poor performance of LAI  
418 DA under dry condition is mainly attributed to the fact that the amount of water in Noah-MP is  
419 conservative. The LAI assimilation in dry condition introduces more vegetation, which requires  
420 more water in the system to replenish the soil water supply. However, the model has no additional  
421 source of water, since the input precipitation is negatively biased.

422 Although a blind bias case (e.g., unknown biases in the precipitation forcing dataset) is  
423 presented here in which the EnKF is run in a sub-optimal mode, the assimilation of LAI  
424 observations is proven useful to improve several model output variables. Future research should  
425 focus on alternative DA methods, such as updating other related model states while assimilating

426 LAI observations, perturbing the model initial condition and model parameters, and/or assimilating  
427 actual satellite-based LAI observations (e.g., MODIS, GLASS) at the global scale to verify the  
428 efficiency of the proposed vegetation DA framework. This may be particularly useful in  
429 agricultural areas, where the vegetation conditions are largely impacted by cropping schedules  
430 (Kumar et al. 2019b). Moreover, future work could investigate multi-variate DA techniques that  
431 combine the assimilation of several variables (such as LAI, soil moisture, and TWS) at the global  
432 scale.

433

434

435

436 ***Acknowledgements:*** This research is sponsored by the NASA Modeling, Analysis, and  
437 Prediction (MAP) Program (80NSSC17K0109). We would also like to acknowledge the  
438 computational resources and support from the ARGO HPC Cluster team at George Mason  
439 University.

440 **References**

- 441 Adegoke, J. O. and Carleton, A. M.: Relations between soil moisture and satellite vegetation  
442 indices in the US Corn Belt, *J. Hydrometeorol.*, 3, 395-405, [https://doi.org/10.1175/1525-7541\(2002\)003<0395:RBSMAS>2.0.CO;2](https://doi.org/10.1175/1525-7541(2002)003<0395:RBSMAS>2.0.CO;2), 2002.
- 444 Albergel, C., Munier, S., Leroux, D.J., Dewaele, H., Fairbairn, D., Barbu, A.L., Gelati, E., Dorigo,  
445 W., Faroux, S., Meurey, C. and Le Moigne, P.: Sequential assimilation of satellite-derived  
446 vegetation and soil moisture products using SURFEX\_v8. 0: LDAS-Monde assessment over  
447 the Euro-Mediterranean area, *Geosci. Model Dev.*, 10, 3889-3912,  
448 <https://doi.org/10.5194/gmd-10-3889-2017>, 2017. Andreadis, K. M. and Lettenmaier, D. P.:  
449 Assimilating remotely sensed snow observations into a macroscale hydrology model, *Adv.*  
450 *Water Resour.*, 29, 872-886, <https://doi.org/10.1016/j.advwatres.2005.08.004>, 2006.
- 451 Arora, V.: Modeling vegetation as a dynamic component in soil - vegetation - atmosphere transfer  
452 schemes and hydrological models, *Rev. Geophys.*, 40, 3-1,  
453 <https://doi.org/10.1029/2001RG000103>, 2002.
- 454 Ball, J. T., Woodrow, I. E. and Berry, J. A.: A model predicting stomatal conductance and its  
455 contribution to the control of photosynthesis under different environmental conditions, in:  
456 *Progress in photosynthesis research*, Springer, Dordrecht, 221-224,  
457 [https://doi.org/10.1007/978-94-017-0519-6\\_48](https://doi.org/10.1007/978-94-017-0519-6_48), 1987.
- 458 Barbu, A. L., Calvet, J. C., Mahfouf, J. F., Albergel, C., and Lafont, S.: Assimilation of Soil  
459 Wetness Index and Leaf Area Index into the ISBA-A-gs land surface model: grassland case  
460 study, *Biogeosciences*, 8, 1971-1986, <https://doi.org/10.5194/bg-8-1971-2011>, 2011.
- 461 Baret, F., Hagolle, O., Geiger, B., Bicheron, P., Miras, B., Huc, M., Berthelot, B., Niño, F., Weiss,  
462 M., Samain, O. and Roujean, J. L.: LAI, fAPAR and fCover CYCLOPES global products  
463 derived from VEGETATION: Part 1: Principles of the algorithm, *Remote Sens. Environ.*, 110,  
464 275-286, <https://doi.org/10.1016/j.rse.2007.02.018>, 2007.
- 465 Cohen, W. B. and Justice, C. O.: Validating MODIS terrestrial ecology products: linking in situ  
466 and satellite measurements, *Remote Sens. Environ.*, 70, 1-3, 1999.
- 467 Cracknell, A. P.: *Advanced very high resolution radiometer AVHRR*, CRC Press, 543, 1997.
- 468 Crow, W. T. and Wood, E. F.: The assimilation of remotely sensed soil brightness temperature  
469 imagery into a land surface model using ensemble Kalman filtering: A case study based on  
470 ESTAR measurements during SGP97, *Adv. Water Resour.*, 26, 137-149,  
471 [https://doi.org/10.1016/S0309-1708\(02\)00088-X](https://doi.org/10.1016/S0309-1708(02)00088-X), 2003.
- 472 De Lannoy, G.J., Reichle, R.H., Arsenault, K.R., Houser, P.R., Kumar, S., Verhoest, N.E. and  
473 Pauwels, V.R.: Multiscale assimilation of Advanced Microwave Scanning Radiometer–EOS  
474 snow water equivalent and Moderate Resolution Imaging Spectroradiometer snow cover  
475 fraction observations in northern Colorado, *Water Resour. Res.*, 48,  
476 <https://doi.org/10.1029/2011WR010588>, 2012
- 477 Di, L., Rundquist, D. C. and Han, L.: Modelling relationships between NDVI and precipitation  
478 during vegetative growth cycles, *Int. J. Remote Sens.*, 15, 2121-2136,  
479 <https://doi.org/10.1080/01431169408954231>, 1994.

480 Dickinson, R. E., Shaikh, M., Bryant, R. and Graumlich, L.: Interactive canopies for a climate  
481 model, *J. Climate*, 11(, 2823-2836, [https://doi.org/10.1175/1520-0442\(1998\)011<2823:ICFACM>2.0.CO;2](https://doi.org/10.1175/1520-0442(1998)011<2823:ICFACM>2.0.CO;2), 1998.

483 Druel, A., Ciais, P., Krinner, G., and Peylin, P.: Modeling the vegetation dynamics of northern  
484 shrubs and mosses in the ORCHIDEE land surface model, *J. Adv. Model Earth Sy.*, 11, 2020-  
485 2035, <https://doi.org/10.1029/2018MS001531>, 2019.

486 Durand, M. and Margulis, S. A.: Effects of uncertainty magnitude and accuracy on assimilation of  
487 multiscale measurements for snowpack characterization, *J. Geophys. Res.: Atmos.*, 113,  
488 D02105, <https://doi.org/10.1029/2007JD008662>, 2008.

489 Evensen, G.: The ensemble Kalman filter: Theoretical formulation and practical implementation,  
490 *Ocean dynam.*, 53, 343-367, <https://doi.org/10.1007/s10236-003-0036-9>, 2003.

491 Fairbairn, D., Barbu, A., Napoly, A., Albergel, C., Mahfouf, J. F., and Calvet, J. C.: The effect of  
492 satellite-derived surface soil moisture and leaf area index land data assimilation on streamflow  
493 simulations over France. *HESS*, 21, 2015-2033, <https://doi.org/10.5194/hess-21-2015-2017>,  
494 2017

495 Farrar, T. J., Nicholson, S. E. and Lare, A. R.: The influence of soil type on the relationships  
496 between NDVI, rainfall, and soil moisture in semiarid Botswana. II. NDVI response to soil  
497 moisture, *Remote Sens. Environ.*, 50, 121-133, [https://doi.org/10.1016/0034-4257\(94\)90039-6](https://doi.org/10.1016/0034-4257(94)90039-6), 1994.

499 Fisher, R. A., Koven, C. D., Anderegg, W. R., Christoffersen, B. O., Dietze, M. C., Farrior, C. E.,  
500 Holm, J. A., Hurtt, G. C., Knox, R. G., Lawrence, P. J. and Lichstein, J. W.: Vegetation  
501 demographics in Earth System Models: A review of progress and priorities, *Global Change*  
502 *Biol.*, 24, 35-54, <https://doi.org/10.1111/gcb.13910>, 2018.

503 Foley, J. A., Prentice, I. C., Ramankutty, N., Levis, S., Pollard, D., Sitch, S. and Haxeltine, A.: An  
504 integrated biosphere model of land surface processes, terrestrial carbon balance, and  
505 vegetation dynamics, *Global Biogeochem. Cy.*, 10, 603-628,  
506 <https://doi.org/10.1029/96GB02692>, 1996.

507 Gelaro, R., McCarty, W., Suárez, M. J., Todling, R., Molod, A., Takacs, L., Randles, C. A.,  
508 Darmenov, A., Bosilovich, M. G., Reichle, R. and Wargan, K.: The modern-era retrospective  
509 analysis for research and applications, version 2 (MERRA-2), *J. Climate*, 30, 5419-5454,  
510 <https://doi.org/10.1175/JCLI-D-16-0758.1>, 2017.

511 Ghatak, D., Zaitchik, B., Kumar, S., Matin, M., Bajracharya, B., Hain, C. and Anderson, M.:  
512 Influence of Precipitation Forcing Uncertainty on Hydrological Simulations with the NASA  
513 South Asia Land Data Assimilation System, *Hydrology*, 5, 57,  
514 <https://doi.org/10.3390/hydrology5040057>, 2018.

515 Gibelin, A. L., Calvet, J. C., Roujean, J. L., Jarlan, L. and Los, S. O.: Ability of the land surface  
516 model ISBA - A - gs to simulate leaf area index at the global scale: Comparison with  
517 satellites products, *J. Geophys. Res.: Atmos.*, 111, D18102,  
518 <https://doi.org/10.1029/2005JD006691>, 2006.

519 Hansen, M. C., DeFries, R. S., Townshend, J. R. and Sohlberg, R.: Global land cover classification  
520 at 1 km spatial resolution using a classification tree approach, *Int. J. Remote Sens.*, 21, 1331-  
521 1364, <https://doi.org/10.1080/014311600210209>, 2000.

522 Justice, C. O., Townshend, J. R. G., Vermote, E. F., Masuoka, E., Wolfe, R. E., Saleous, N., Roy,  
523 D. P. and Morisette, J. T.: An overview of MODIS Land data processing and product status,  
524 Remote Sens. Environ., 83, 3-15, [https://doi.org/10.1016/S0034-4257\(02\)00084-6](https://doi.org/10.1016/S0034-4257(02)00084-6), 2002.

525 Kim, Y. and Wang, G.: Impact of vegetation feedback on the response of precipitation to  
526 antecedent soil moisture anomalies over North America J. Hydrometeorol., 8, 534-550,  
527 <https://doi.org/10.1175/JHM612.1>, 2007.

528 Krinner, G., Viovy, N., de Noblet - Ducoudré, N., Ogée, J., Polcher, J., Friedlingstein, P., Ciais,  
529 P., Sitch, S. and Prentice, I. C.: A dynamic global vegetation model for studies of the coupled  
530 atmosphere - biosphere system, Global Biogeochem. Cy., 19, GB1015,  
531 <https://doi.org/10.1029/2003GB002199>, 2005.

532 Kucharik, C. J., Foley, J. A., Delire, C., Fisher, V. A., Coe, M. T., Lenters, J. D., Young - Molling,  
533 C., Ramankutty, N., Norman, J. M. and Gower, S. T.: Testing the performance of a dynamic  
534 global ecosystem model: water balance, carbon balance, and vegetation structure, Global  
535 Biogeochem. Cy., 14, 795-825, <https://doi.org/10.1029/1999GB001138>, 2000.

536 Kumar, S. V., Peters-Lidard, C. D., Tian, Y., Houser, P. R., Geiger, J., Olden, S., Lighty, L.,  
537 Eastman, J. L., Doty, B., Dirmeyer, P. and Adams, J.: Land information system: An  
538 interoperable framework for high resolution land surface modeling, Environ. Modell. Softw.,  
539 21, 1402-1415, <https://doi.org/10.1016/j.envsoft.2005.07.004>, 2006.

540 Kumar, S. V., Peters-Lidard, C., Tian, Y., Reichle, R., Geiger, J., Alonge, C., Eylander, J. and  
541 Houser, P.: An integrated hydrologic modeling and data assimilation framework, Computer,  
542 41, 52-59, <https://doi.org/10.1109/MC.2008.475>, 2008.

543 Kumar, S. V., Peters-Lidard, C. D., Mocko, D., Reichle, R., Liu, Y., Arsenault, K. R., Xia, Y., Ek,  
544 M., Riggs, G., Livneh, B. and Cosh, M.: Assimilation of remotely sensed soil moisture and  
545 snow depth retrievals for drought estimation, J. Hydrometeorol., 15, 2446-2469,  
546 <https://doi.org/10.1175/JHM-D-13-0132.1>, 2014.

547 Kumar, S.V., Zaitchik, B.F., Peters-Lidard, C.D., Rodell, M., Reichle, R., Li, B., Jasinski, M.,  
548 Mocko, D., Getirana, A., De Lannoy, G. and Cosh, M.H.: Assimilation of gridded GRACE  
549 terrestrial water storage estimates in the North American Land Data Assimilation System, J.  
550 Hydrometeorol., 17, 1951-1972, <https://doi.org/10.1175/JHM-D-15-0157.1>, 2016

551 Kumar, S. V., Jasinski, M., Mocko, D. M., Rodell, M., Borak, J., Li, B., Beaudoin, H. K. and  
552 Peters-Lidard, C. D.: NCA-LDAS land analysis: Development and performance of a  
553 multisensor, multivariate land data assimilation system for the National Climate Assessment,  
554 J. Hydrometeorol., 20, 1571-1593, <https://doi.org/10.1175/JHM-D-17-0125.1>, 2019.

555 Kumar, S. V., Mocko, D. M., Wang, S., Peters-Lidard, C. D. and Borak, J.: Assimilation of  
556 remotely sensed Leaf Area Index into the Noah-MP land surface model: Impacts on water and  
557 carbon fluxes and states over the Continental US, J. Hydrometeorol., 20, 1359-1377,  
558 <https://doi.org/10.1175/JHM-D-18-0237.1>, 2019.

559 Ling, X. L., Fu, C. B., Guo, W. D. and Yang, Z. L.: Assimilation of remotely sensed LAI into  
560 CLM4CN using DART, J. Adv. Model. Earth Sy., <https://doi.org/10.1029/2019MS001634>,  
561 2019.

562 Liu, Y., Liu, R. and Chen, J. M.: Retrospective retrieval of long - term consistent global leaf area  
563 index (1981 - 2011) from combined AVHRR and MODIS data, *J. Geophys. Res.: Biogeo.*,  
564 117, G04003, <https://doi.org/10.1029/2012JG002084>, 2012.

565 Liu, Y., Peters - Lidard, C.D., Kumar, S.V., Arsenault, K.R. and Mocko, D.M.: Blending  
566 satellite - based snow depth products with in situ observations for streamflow predictions in  
567 the Upper Colorado River Basin, *Water Resour. Res.*, 51, 1182-1202,  
568 <https://doi.org/10.1002/2014WR016606>, 2015

569 Morisette, J. T., Privette, J. L. and Justice, C. O.: A framework for the validation of MODIS land  
570 products, *Remote Sens. Environ.*, 83, 77-96, [https://doi.org/10.1016/S0034-4257\(02\)00088-](https://doi.org/10.1016/S0034-4257(02)00088-3)  
571 3, 2002.

572 Myneni, R. B., Hoffman, S., Knyazikhin, Y., Privette, J. L., Glassy, J., Tian, Y., Wang, Y., Song,  
573 X., Zhang, Y., Smith, G. R. and Lotsch, A.: Global products of vegetation leaf area and  
574 fraction absorbed PAR from year one of MODIS data, *Remote Sens. Environ.*, 83, 214-231,  
575 [https://doi.org/10.1016/S0034-4257\(02\)00074-3](https://doi.org/10.1016/S0034-4257(02)00074-3), 2002.

576 Niu, G. Y. and Yang, Z. L.: An observation - based formulation of snow cover fraction and its  
577 evaluation over large North American river basins, *J. Geophys. Res.: Atmos.*, 112, D21101,  
578 <https://doi.org/10.1029/2007JD008674>, 2007.

579 Niu, G. Y., Yang, Z. L., Mitchell, K. E., Chen, F., Ek, M. B., Barlage, M., Kumar, A., Manning,  
580 K., Niyogi, D., Rosero, E. and Tewari, M.: The community Noah land surface model with  
581 multiparameterization options (Noah - MP): 1. Model description and evaluation with local -  
582 scale measurements, *J. Geophys. Res.: Atmos.*, 116, D12109,  
583 <https://doi.org/10.1029/2010JD015139>, 2011.

584 Pagano, T. S. and Durham, R. M.: Moderate resolution imaging spectroradiometer (MODIS), in:  
585 Proceedings of SPIE 1939 Sensor Systems for the Early Earth Observing System Platforms,  
586 International Society for Optics and Photonics, Orlando, FL, United States, 25 August 1993,  
587 2-17, <https://doi.org/10.1117/12.152835>, 1993

588 Pan, M. and Wood, E. F.: Data assimilation for estimating the terrestrial water budget using a  
589 constrained ensemble Kalman filter, *J. Hydrometeorol.*, 7, 534-547,  
590 <https://doi.org/10.1175/JHM495.1>, 2006.

591 Pauwels, V. R. and De Lannoy, G. J.: Improvement of modeled soil wetness conditions and  
592 turbulent fluxes through the assimilation of observed discharge, *J. Hydrometeorol.*, 7, 458-  
593 477, <https://doi.org/10.1175/JHM490.1>, 2006.

594 Pauwels, V. R., Verhoest, N. E., De Lannoy, G. J., Guissard, V., Lucau, C. and Defourny, P.:  
595 Optimization of a coupled hydrology-crop growth model through the assimilation of observed  
596 soil moisture and leaf area index values using an ensemble Kalman filter, *Water Resour. Res.*,  
597 43, W04421, <https://doi.org/10.1029/2006WR004942>, 2007.

598 Peters-Lidard, C. D., Houser, P. R., Tian, Y., Kumar, S. V., Geiger, J., Olden, S., Lighty, L., Doty,  
599 B., Dirmeyer, P., Adams, J. and Mitchell, K. High-performance Earth system modeling with  
600 NASA/GSFC's Land Information System, *Innovations Syst. Softw. Eng.*, 3, 157-165,  
601 <https://doi.org/10.1007/s11334-007-0028-x>, 2007.



602 Privette, J. L., Myneni, R. B., Knyazikhin, Y., Mukelabai, M., Roberts, G., Tian, Y., Wang, Y. and  
603 Leblanc, S. G.: Early spatial and temporal validation of MODIS LAI product in the Southern  
604 Africa Kalahari, *Remote Sens. Environ.*, 83, 232-243, [https://doi.org/10.1016/S0034-](https://doi.org/10.1016/S0034-4257(02)00075-5)  
605 [4257\(02\)00075-5](https://doi.org/10.1016/S0034-4257(02)00075-5), 2002.

606 Reichle, R. H., McLaughlin, D. B. and Entekhabi, D.: Hydrologic data assimilation with the  
607 ensemble Kalman filter, *Mon. Weather Rev.*, 130, 103-114, [https://doi.org/10.1175/1520-](https://doi.org/10.1175/1520-0493(2002)130<0103:HDAWTE>2.0.CO;2)  
608 [0493\(2002\)130<0103:HDAWTE>2.0.CO;2](https://doi.org/10.1175/1520-0493(2002)130<0103:HDAWTE>2.0.CO;2), 2002.

609 Reichle, R. H., Walker, J. P., Koster, R. D. and Houser, P. R.: Extended versus ensemble Kalman  
610 filtering for land data assimilation, *J. Hydrometeorol.*, 3, 728-740,  
611 [https://doi.org/10.1175/1525-7541\(2002\)003<0728:EVEKFF>2.0.CO;2](https://doi.org/10.1175/1525-7541(2002)003<0728:EVEKFF>2.0.CO;2), 2002.

612 Reichle, R. H., Koster, R. D., Liu, P., Mahanama, S. P., Njoku, E. G. and Owe, M.: Comparison  
613 and assimilation of global soil moisture retrievals from the Advanced Microwave Scanning  
614 Radiometer for the Earth Observing System (AMSR - E) and the Scanning Multichannel  
615 Microwave Radiometer (SMMR), *J. Geophys. Res.: Atmos.*, 112, D09108,  
616 <https://doi.org/10.1029/2006JD008033>, 2007.

617 Reichle, R. H., Kumar, S. V., Mahanama, S. P., Koster, R. D. and Liu, Q.: Assimilation of satellite-  
618 derived skin temperature observations into land surface models, *J. Hydrometeorol.*, 11, 1103-  
619 1122, <https://doi.org/10.1175/2010JHM1262.1>, 2010.

620 Richard, Y. and Pocard, I.: A statistical study of NDVI sensitivity to seasonal and interannual  
621 rainfall variations in Southern Africa, *Int. J. Remote Sens.*, 19, 2907-2920,  
622 <https://doi.org/10.1080/014311698214343>, 1998.

623 Sabater, J. M., Rüdiger, C., Calvet, J. C., Fritz, N., Jarlan, L. and Kerr, Y.: Joint assimilation of  
624 surface soil moisture and LAI observations into a land surface model, *Agr. Forest Meteorol.*,  
625 148, 1362-1373, <https://doi.org/10.1016/j.agrformet.2008.04.003>, 2008.

626 Tian, Y., Woodcock, C. E., Wang, Y., Privette, J. L., Shabanov, N. V., Zhou, L., Zhang, Y.,  
627 Buermann, W., Dong, J., Veikkanen, B. and Häme, T.: Multiscale analysis and validation of  
628 the MODIS LAI product: I. Uncertainty assessment, *Remote Sens. Environ.*, 83, 414-430,  
629 [https://doi.org/10.1016/S0034-4257\(02\)00047-0](https://doi.org/10.1016/S0034-4257(02)00047-0), 2002.

630 Wang, G. and Eltahir, E. A.: Role of vegetation dynamics in enhancing the low - frequency  
631 variability of the Sahel rainfall, *Water Resour. Res.*, 36, 1013-1021,  
632 <https://doi.org/10.1029/1999WR900361>, 2000.

633 Wang, G., Sun, S. and Mei, R.: Vegetation dynamics contributes to the multi - decadal variability  
634 of precipitation in the Amazon region, *Geophys. Res. Lett.*, 38, L19703,  
635 <https://doi.org/10.1029/2011GL049017>, 2011.

636 Woodward, F. I. and Lomas, M. R.: Vegetation dynamics—simulating responses to climatic change,  
637 *Biol. Rev.*, 79, 643-670, <https://doi.org/10.1017/S1464793103006419>, 2004.

638 Xiao, Z., Liang, S., Wang, J., Chen, P., Yin, X., Zhang, L. and Song, J. Use of general regression  
639 neural networks for generating the GLASS leaf area index product from time-series MODIS  
640 surface reflectance, *IEEE T. Geosci. Remote*, 52, 209-223,  
641 <https://doi.org/10.1109/TGRS.2013.2237780>, 2013.

- 642 Yang, Z. L., Niu, G. Y., Mitchell, K. E., Chen, F., Ek, M. B., Barlage, M., Longuevergne, L.,  
643 Manning, K., Niyogi, D., Tewari, M. and Xia, Y.: The community Noah land surface model  
644 with multiparameterization options (Noah - MP): 2. Evaluation over global river basins, J.  
645 Geophys. Res.: Atmos., 116, D12110, <https://doi.org/10.1029/2010JD015140>, 2011.
- 646 Yoon, Y., Kumar, S.V., Forman, B.A., Zaitchik, B.F., Kwon, Y., Qian, Y., Rupper, S., Maggioni,  
647 V., Houser, P., Kirschbaum, D. and Richey, A.: Evaluating the uncertainty of terrestrial water  
648 budget components over High Mountain Asia, Front. Earth Sci., 7,  
649 <https://doi.org/10.3389/feart.2019.00120>, 2019
- 650 Zhou, Y., McLaughlin, D. and Entekhabi, D.: Assessing the performance of the ensemble Kalman  
651 filter for land surface data assimilation, Mon. Weather Rev., 134, 2128-2142,  
652 <https://doi.org/10.1175/MWR3153.1>, 2006.